Enhanced canopy growth precedes senescence in 2005 and 2010 Amazonian droughts

Yi Y. Liu[1*], Albert I.J.M. van Dijk[2], Diego G. Miralles[3], Matthew F. McCabe[4], Jason P. Evans[5], Richard A.M. de Jeu[6], Pierre Gentine[7], Alfredo Huete[8], Robert M. Parinussa[1], Lixin Wang[9], Kaiyu Guan[10], Joe Berry[11], Natalia Restrepo-Coupe[8]

[1]School of Geographical Sciences, Nanjing University of Information Science and Technology, Nanjing, 210044, China.

[2]Fenner School of Environment & Society, Australian National University, Canberra, Australian Capital Territory 0200, Australia.

[3]Laboratory of Hydrology and Water Management, Ghent University, Ghent 9000, Belgium.

[4]Division of Biological and Environmental Sciences and Engineering, King Abdullah University of Science and Technology, Thuwal 23955-6900, Saudi Arabia.

[5]ARC Centre of Excellence for Climate Extremes & Climate Change Research Centre, University of New South Wales, Sydney, New South Wales 2052, Australia.

[6]VanderSat B.V., Wilhelminastraat 43A, 2011 VK, Haarlem, Netherlands.

[7]Department of Earth and Environmental Engineering and Earth Institute, Columbia University, New York, NY 10027, USA.

[8]Climate Change Cluster (C3), University of Technology Sydney, Sydney, New South Wales 2007, Australia.

[9]Department of Earth Sciences, Indiana University-Purdue University Indianapolis (IUPUI), Indianapolis, Indiana 46202, USA.

This is the author's manuscript of the article published in final edited form as:
Liu, Y. Y., van Dijk, A. I. J. M., Miralles, D. G., McCabe, M. F., Evans, J. P., de Jeu, R. A. M., … Restrepo-Coupe, N. (2018). Enhanced canopy growth precedes senescence in 2005 and 2010 Amazonian droughts. Remote Sensing of Environment, 211, 26–37. https://doi.org/10.1016/j.rse.2018.03.035

[10]Department of Natural Resources and Environmental Sciences and National Center for Supercomputing Applications, University of Illinois at Urbana Champaign, Urbana, Illinois 61801, USA

[11]Department of Global Ecology, Carnegie Institution of Washington, 260 Panama Street Stanford, California 94305, USA

Corresponding author:

Yi Y. Liu

yiliu001@gmail.com

+86-25-58235190

Abstract

Unprecedented droughts hit southern Amazonia in 2005 and 2010, causing a sharp increase in tree mortality and carbon loss. To better predict the rainforest's response to future droughts, it is necessary to understand its behavior during past events. Satellite observations provide a practical source of continuous observations of Amazonian forest. Here we used a passive microwave-based vegetation water content record (i.e., vegetation optical depth, VOD), together with multiple hydrometeorological observations as well as conventional satellite vegetation measures, to investigate the rainforest canopy dynamics during the 2005 and 2010 droughts. During the onset of droughts in the wet-to-dry season (May–July) of both years, we found large-scale positive anomalies in VOD, leaf area index (LAI) and enhanced vegetation index (EVI) over the southern Amazonia. These observations are very likely caused by enhanced canopy growth. Concurrent below-average rainfall and above-average radiation during the wet-to-dry season can be interpreted as an early arrival of normal dry season conditions, leading to enhanced new leaf development and ecosystem photosynthesis, as supported by field observations. Our results suggest that further rainfall deficit into the subsequent dry season caused water and heat stress during the peak of 2005 and 2010 droughts (August–October) that exceeded the tolerance limits of the rainforest, leading to widespread negative VOD anomalies over the southern Amazonia. Significant VOD anomalies were observed mainly over the western part in 2005 and mainly over central and eastern parts in 2010. The total area with significant negative VOD anomalies was comparable between these two drought years, though the average magnitude of significant negative VOD anomalies was greater in 2005. This finding broadly agrees with the field

observations indicating that the reduction in biomass carbon uptake was stronger in 2005 than 2010. The enhanced canopy growth preceding drought-induced senescence should be taken into account when interpreting the ecological impacts of Amazonian droughts.

Keywords:

Amazonian Droughts, Canopy Water Content, Satellite, Passive Microwave, Soil Water Deficit, Surface Temperature, Vapor Pressure Deficit

1. Introduction

The Amazonian rainforest plays a critical role in the global hydrological and carbon cycles (Pan *et al.*, 2011). However, over the last decades, droughts over Amazonia have intensified (Marengo & Espinoza, 2016), with a once-in-a-century drought in 2005 followed by even more severe droughts in 2010 (Lewis *et al.*, 2011) and 2015 (Jiménez-Muñoz *et al.*, 2016). These large-scale droughts resulted in unprecedented low river discharges (Xu *et al.*, 2011), increased tree mortality (Phillips *et al.*, 2009) and a reversal of a large and long-term net carbon uptake (Doughty *et al.*, 2015, Feldpausch *et al.*, 2016, Gatti *et al.*, 2014, Lewis *et al.*, 2011).

To better anticipate Amazonian rainforest response to severe droughts in the future and the associated influence on the carbon cycle, it is important to characterize and understand its forest dynamic behavior during the 2005 and 2010 droughts. A long-term research network, RAINFOR, has been monitoring more than 100 forest plots across Amazonia over several decades. These field observations suggest that increased tree mortality in 2005 was the main cause for reduced carbon uptake and was strongly related to drought severity (Phillips *et al.*, 2009). In the 2010 drought, Feldpausch *et al.* (2016) found that a combination of increased tree mortality and slow tree growth was the primary reason for reduced carbon uptake, but the distribution of increased tree mortality in 2010 seemed unrelated to local precipitation anomalies and independent of local pre-2010 drought history. Furthermore, rainfall deficit in 2010 occurred over a larger area than in 2005 (Phillips *et al.*, 2009), but the overall reduction in carbon uptake was greater in 2005 (Feldpausch *et al.*, 2016). Comparing the hydrometeorological conditions and forest dynamics in 2005 and 2010 should contribute to a

96 better understanding of different Amazonian rainforest responses during these two droughts.

97 In addition to field studies, vegetation properties derived by different remote sensing
98 techniques have also been used to investigate Amazonian rainforest responses during the two
99 droughts. Two vegetation indices derived from the optical Moderate Resolution Imaging
100 Spectroradiometer (MODIS), the Normalized Difference Vegetation Index (NDVI) and the
101 Enhanced Vegetation Index (EVI), have extensively been used to characterize rainforest
102 canopy greenness. Widespread below-average canopy greenness was observed in the dry
103 season (July–September) during the 2010 drought from NDVI and EVI (Atkinson *et al.*, 2011,
104 Xu *et al.*, 2011), but there is debate about the canopy greenness anomalies in the 2005 dry
105 season (Saleska *et al.*, 2007, Samanta *et al.*, 2010). Interpretation of these optical sensor
106 observations is challenging as they are strongly influenced by sun-sensor geometry changes and
107 atmospheric effects, e.g., clouds and aerosols (Morton *et al.*, 2014, Saleska *et al.*, 2016,
108 Samanta *et al.*, 2010). Over southern Amazonia, the aerosol concentration was extremely high
109 during the 2005 and 2010 dry season due to large-scale biomass burning (Ten Hoeve *et al.*,
110 2012), which makes it difficult to obtain reliable optical sensor observations of the vegetation
111 canopy.

112 Satellite-based sun-induced chlorophyll fluorescence (SIF) and active microwave (i.e., radar)
113 observations were also explored to understand Amazon drought responses (Lee *et al.*, 2013b,
114 Saatchi *et al.*, 2012). Lee *et al.* (2013b) utilized the SIF measured by the Greenhouse gases
115 Observing SATallite (GOSAT) launched in January 2009. SIF was reduced by 15% across
116 Amazonia during the extended dry season of 2010 compared with the non-drought year 2009.
117 Saatchi *et al.* (2012) used the radar backscatter at microwave frequency (13.4 GHz) from the

SeaWinds Scatterometer onboard QuickSCAT (QSCAT, launched in June 1999 and deactivated in November 2009). An advantage of active microwave sensor observations is that they are minimally affected by clouds and aerosols. They found a strong negative anomaly in the radar backscatter over southwestern Amazonia during the 2005 drought, indicating impacts on the canopy structure and a decline in canopy moisture. Despite the importance of these studies, neither covers both the 2005 and 2010 droughts.

The passive microwave-based vegetation optical depth (VOD) (Owe *et al.*, 2001), derived from 6.9 GHz observations by the Advanced Microwave Scanning Radiometer – Earth Observing System (AMSR-E, June 2002 – October 2011) onboard NASA's Aqua Satellite, covers both 2005 and 2010 droughts, and can represent the canopy water content dynamics over closed-canopy Amazonian rainforest, including leaf and branches components (Andela *et al.*, 2013, Jones *et al.*, 2013, Liu *et al.*, 2015). The advantages of passive microwave-based VOD include that the signal remains sensitive to variations at a relatively high biomass density (Zhou *et al.*, 2014); that, similarly to radar, it is minimally affected by clouds and aerosols, which are very frequent in Amazonia; and that it is less affected by sun-sensor geometry issues, as it relies on natural microwave emission from the Earth rather than reflected sunlight.

The field observations suggest the mechanisms for reduced carbon uptake in rainforests were different in 2005 and 2010 droughts (Feldpausch *et al.*, 2016). Therefore, the primary objective of this study is to analyze the spatiotemporal evolution of these two droughts based on the passive microwave-based AMSR-E VOD and a series of satellite-based hydrometerological observations and identify their unique characteristics to better understand the similarities and differences in Amazonian rainforest responses between 2005 and 2010 events. Specifically, the

rainforest canopy anomalies from satellite observations during both droughts are investigated together with the hydrometeorological variables over the extended dry season (May – October), which covers both the drought onset and peak periods.

2. Materials and Methods

2.1 Satellite-based datasets

We utilized several independent sources of satellite data to characterize vegetation and hydrometeorological dynamics over Amazonia (see Table 1). All data cover the same period from January 2003 through December 2010. The focus is on the dynamics of intact rainforest during 2005 and 2010 droughts. The 0.05 °MODIS land cover product (MCD12C1, v051) based on the International Geosphere-Biosphere Programme (IGBP) classification scheme (Friedl *et al.*, 2010) for the year 2010 was used to delineate the spatial distribution of Amazonian forests (see Fig. 1a).

A new source of vegetation data used here is the passive microwave-based vegetation optical depth (VOD) at 0.10 °spatial resolution. The VOD data were obtained based on brightness temperature derived from C-band (6.9 GHz) and Ka-band (36.5 GHz) observations by the Advanced Microwave Scanning Radiometer – Earth Observing System (AMSR-E) onboard the Aqua satellite. These were retrieved using the Land Parameter Retrieval Model (LPRM) (Meesters *et al.*, 2005, Owe *et al.*, 2008, Owe *et al.*, 2001). The smoothing filter-based intensity modulation (SFIM) approach was utilized to downscale brightness temperature to 0.10 °spatial resolution (Santi, 2010), and then the downscaled brightness temperature was used as the input to LPRM (de Jeu *et al.*, 2014, Parinussa *et al.*, 2014). The VOD is a

dimensionless variable and can be interpreted as being directly proportional to the total vegetation water content, but varying with wavelength, vegetation structure and viewing angle (Jackson & Schmugge, 1991, Kerr & Njoku, 1990, Kirdyashev *et al.*, 1979). Over closed canopy rainforest, the C-band VOD retrievals can be assumed to represent water content dynamics at the canopy level, including the leaves and branches (Guglielmetti *et al.*, 2007, Jones *et al.*, 2011, Jones *et al.*, 2014).

An important assumption in the LPRM approach is that canopy surface temperature is equal to soil surface temperature (Meesters *et al.*, 2005, Owe *et al.*, 2008, Owe *et al.*, 2001). The minimal temperature gradients during the night are therefore more favorable for the retrieval, while the uncertainty is expected to be higher for the day-time overpasses. AMSR-E has daily descending (01:30 equatorial local crossing time) and ascending (13:30 equatorial local crossing time) overpasses. The VOD retrievals from both night- and day-time overpasses were used in this study, with the emphasis on the night-time VOD. Hereafter VOD represent retrievals from night-time overpasses, except where specified otherwise. Optical satellite vegetation data were also used to characterize canopy dynamics, including LAI and EVI. LAI is defined as the one-sided green leaf area per unit ground area. The LAI product used is the latest version (Collection 6) of MODIS from Terra and Aqua combined (Yan *et al.*, 2016a, Yan *et al.*, 2016b). For EVI, the Multi-Angle Implementation of Atmospheric Correction (MAIAC, Collection 6) MODIS product was used. Advantages of the MAIAC data are that they received more sophisticated atmospheric correction, more accurate and less conservative cloud detection, improved sensor calibration, and sun-sensor geometry correction (Bi *et al.*, 2016, Lyapustin *et al.*, 2011a, Lyapustin *et al.*, 2011b, Lyapustin *et al.*, 2012). These data

represent the state-of-the-art in accounting for aerosol and bidirectional reflectance distribution function (BRDF) effects, but some noise may still exist (Bi *et al.*, 2016).

The hydrometeorological variables used here include (1) rainfall (P) from the Tropical Rainfall Measuring Mission (TRMM 3B43 v7) (Huffman *et al.*, 2007), (2) photosynthetically active radiation (PAR) from the Clouds and Earth's Radiant Energy System (CERES, SYN1deg Ed3A) on Aqua and Terra combined (Wielicki *et al.*, 1996), (3) terrestrial water storage (TWS) dynamics estimated by removing the signals of other geophysical processes from the gravity field measured from the Gravity Recovery and Climate Experiment (GRACE) (Landerer & Swenson, 2012, Swenson & Wahr, 2006) , (4) land surface temperature (LST) from the daytime overpass (1:30 PM) of the Atmospheric Infrared Sounder (AIRS) onboard Aqua (version 6). Aerosol optical depth (AOD) and cloud optical thickness (COT) from the Terra MODIS instrument (Platnick *et al.*, 2015) were used to characterize atmospheric conditions. In addition, near surface air temperature (T_a) and surface relative humidity (RH) from both the daytime and nighttime overpasses (1:30 PM and 1:30 AM, respectively) of the Atmospheric Infrared Sounder (AIRS) (version 6) were used to calculate vapor pressure deficit (VPD, see the section below).

2.2 Data pre-processing

For a more direct comparison, data were resampled to a monthly and 0.10 °resolution by aggregation or bilinear interpolation from their original resolutions. To minimize the influence of non-forest vegetation dynamics, the Amazonian forests are defined here as the 0.10 °grid cells in which all four 0.05 °grid cells have the same evergreen broadleaf forest land cover type (Fig. 1a). The presence of large-scale open water affects microwave emissions (Liu *et al.*,

2013). Therefore, the grid cells alongside the Amazon River (obtained from Digital Chart of the World) were masked out before analyzing VOD. Figure 1b shows that average VOD values over forests are generally greater than 0.9; we considered that the signal in grid cells with VOD < 0.9 was influenced by the presence of open water, hence these grid cells were excluded from the analysis.

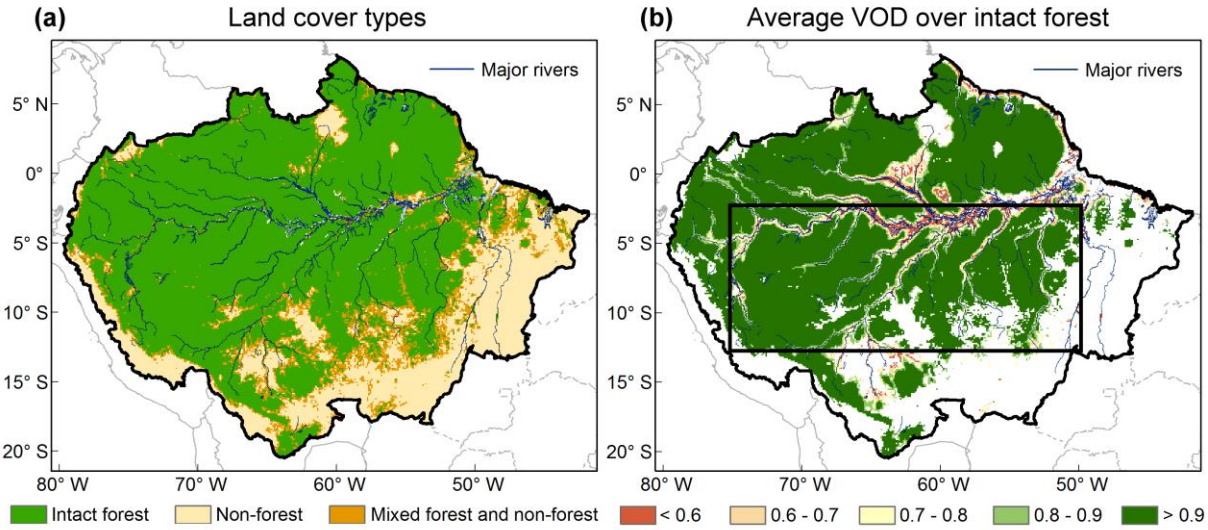

Fig 1. Spatial distribution of vegetation characteristics over the study area. (a) Land cover map (at 0.10 °spatial resolution) over Amazonia based on the 0.05 °MODIS IGBP classification product for 2010. 'Intact forest' means that all four 0.05° grid cells in one 0.10 ° grid cell are classified as forest. (b) The 'intact forest' in southern Amazonia (2.5°S–12.5 °S, 75 °W–50 °W as outlined) is the study area of this paper. The annual average VOD value at 0.10 °spatial resolution is displayed in the background. A brief comparison between the downscaled (0.10 °) and original (0.25 °) VOD data can be found in Fig. S1.

Atmospheric VPD is the difference between the theoretical pressure corresponding to saturated water vapor in the air (e_s) and the actual pressure of water vapor in the air (e_a); it is a measure of the evaporative demand of the atmosphere. Higher VPD reflects higher

atmospheric moisture demand (Seager *et al.*, 2015), and this can exacerbate physiological stress on vegetation under drought conditions, thereby reducing the photosynthesis (Jarvis 1976, Leuning 1995). The AIRS-based near surface air temperature (T_a) represents observations around 1:30 PM and 1:30 AM, close to the maximum and minimum daily surface air temperature, respectively (i.e., T_{aMAX} and T_{aMIN} in ℃). Accordingly, surface relative humidity (RH, %) observations around 1:30 PM and 1:30 AM should be close to the minimum and maximum daily RH as well (i.e., RH_{MIN} and RH_{MAX}). The VPD (in kPa) is calculated as $e_s - e_a$, where:

$$e_s = [e^o(T_{aMAX}) + e^o(T_{aMIN})] / 2 \quad (1)$$

$$e^o(T_{aMAX}) = 0.6108 \times \exp[17.27 \times T_{aMAX} / (T_{aMAX} + 237.3)] \quad (2)$$

$$e^o(T_{aMIN}) = 0.6108 \times \exp[17.27 \times T_{aMIN} / (T_{aMIN} + 237.3)] \quad (3)$$

$$e_a = [e^o(T_{aMAX}) \times (RH_{MIN} / 100) + e^o(T_{aMIN}) \times (RH_{MAX} / 100)] / 2 \quad (4)$$

2.3 Analysis Methods

First, we examined the temporal evolution of hydrometeorological conditions over southern Amazonia. The seasonal cycle of hydrometeorological variables over southern Amazonia in non-drought years was calculated by taking the average for 2003–2010 but excluding 2005 and 2010, for P, PAR, AOD, COT, TWS, LST and VPD. The anomalies of these variables during the extended dry season (May–October) in 2005 and 2010 were calculated with respect to the seasonal cycle of non-drought years. In addition, TWS represents a vertically-integrated sum of all water stores, including ground water, soil moisture, surface water and vegetation water. In non-drought years, when TWS reaches its minimum value during the dry season

(referred to as TWS_{MIN}) (Guan *et al.*, 2015), the sap flow and transpiration can remain at a high level, and there is little evidence for limitation of water use (Fisher *et al.*, 2006, 2007). New leaf development and ecosystem photosynthesis increase during the dry season according to field observations (Wu *et al.*, 2016). However, under drought conditions, soil moisture falls below the dry-season level for non-drought years, and sap flow is substantially reduced due to water limitation (Fisher *et al.*, 2006, 2007). As such, we consider TWS_{MIN} as a threshold level: when $TWS>TWS_{MIN}$, sufficient water storage is assumed to be available for vegetation water demand, and when $TWS<TWS_{MIN}$, water deficit is assumed to occur. Likewise, LST_{MAX} and VPD_{MAX}, which represent the maximum values of LST and VPD during the dry season of non-drought years, are also used as thresholds. The differences between the actual values in drought years and TWS_{MIN}, LST_{MAX} and VPD_{MAX} were calculated for each grid cell during the onset and peak of droughts, to represent the temporal and spatial patterns of water deficit and heat stress.

For the vegetation indices (including VOD, EVI and LAI), standardized anomalies were calculated for a direct comparison with each other. For each grid cell, the anomaly represents the departure from the average for the same months within the reference period. These values were standardized by division over the corresponding standard deviation within the reference period. Here the reference period is 2003–2010 but excluding 2005 and 2010.

The non-parametric Wilcoxon signed rank test (Gibbons & Chakraborti, 2011) was used to calculate the statistical significance of the anomalies. In this study, this test was first used to identify the grid cells over which the anomalies during droughts are statistically different from non-drought years at $p<0.05$. It was also used to determine whether the anomalies between 2005 and 2010 events were statistically different at $p<0.05$.

Potential evapotranspiration is estimated to be around 100 mm per month over Amazonia with relatively small variations between dry and wet seasons (Aragao *et al.*, 2007, Guan *et al.*, 2015). It is normal for monthly rainfall to drop below 100 mm in the dry season of non-drought years. Here we considered months which received rainfall below 100 mm and also significantly (p<0.05) below the average for non-drought years, which is expected to cause soil moisture depletion. To delineate the severity of soil moisture stress, the total number of months with rainfall below 100 mm and significantly (p<0.05) below average was calculated between May and October in 2005 and 2010 for each grid cell.

273 **Table 1**. List of satellites datasets used in this study

Dataset	Sensor/ Platform	Original spatial resolution	Sources
Vegetation characteristics			
Land Cover Type	MODIS/ Terra and Aqua	0.05 °	http://e4ftl01.cr.usgs.gov/MOTA/MCD12C1.051/2010.01.01 (‘IGBP global vegetation classification scheme’)
Vegetation Optical Depth (VOD)	AMSR-E/ Aqua	0.10 ° (~10km)	Derived using the LPRM algorithm and the SFIM downscaling technique, and VOD data available upon request
Leaf Area Index (LAI)	MODIS/ Terra and Aqua	0.5km	https://e4ftl01.cr.usgs.gov/MOTA/MCD15A2H.006 MCD15A2H (V006)
Enhanced Vegetation Index (EVI)	MODIS/ Terra and Aqua	1km	ftp://dataportal.nccs.nasa.gov/DataRelease/SouthAmerica/VI (MAIAC Collection 6)
Hydrometeorological variables			
Rainfall (P)	TRMM and other satellites	0.25 °	ftp://disc2.nascom.nasa.gov/ftp/data/s4pa/TRMM_L3/TRMM_3B43 (TRMM 3B43 v7)
Photosynthetically Active Radiation (PAR)	CERES/ Terra and Aqua	1 °	https://ceres-tool.larc.nasa.gov/ord-tool/jsp/SYN1degSelection.jsp (PAR Surface Flux Direct' and PAR Surface Flux Diffuse')
Aerosol Optical Depth (AOD)	MODIS/ Terra	1 °	https://ladsweb.modaps.eosdis.nasa.gov/archive/allData/6/MOD08_M3 (‘Aerosol_Optical_Depth_Land_Ocean_Mean_Mean’)
Cloud Optical Thickness (COT)	MODIS/ Terra	1 °	https://ladsweb.modaps.eosdis.nasa.gov/archive/allData/6/MOD08_M3 (‘Cloud_Optical_Thickness_Combined_Mean_Mean’)
Terrestrial Water Storage (TWS)	GRACE	1 °	ftp://podaac-ftp.jpl.nasa.gov/allData/tellus/L3/land_mass/RL05 (RL05.DSTvSCS1401, simple arithmetic mean of JPL, CSR and GFZ fields used)
Surface Skin Temperature (LST)	AIRS/ Aqua	1 °	ftp://acdisc.sci.gsfc.nasa.gov/data/s4pa/Aqua_AIRS_Level3 ('SurfSkinTemp_A') ‘A’ representing ascending overpasses with equatorial crossing time 1:30PM
Surface Air Temperature (T_a)	AIRS/ Aqua	1 °	ftp://acdisc.sci.gsfc.nasa.gov/data/s4pa/Aqua_AIRS_Level3 ('SurfAirTemp_A' and 'SurfAirTemp_D') ‘D’ representing ascending overpasses with equatorial crossing time 1:30AM
Surface Relative Humidity (RH)	AIRS/ Aqua	1 °	ftp://acdisc.sci.gsfc.nasa.gov/data/s4pa/Aqua_AIRS_Level3 ('RelHumSurf_A' and ' RelHumSurf _D')

3. Results and Discussion

3.1 Hydrometeorological anomalies in 2005 and 2010 droughts

Over southern Amazonia (2.5–12.5 °S, 50–75 °W, Fig. 1b), there is a strong seasonal cycle in rainfall (P) and photosynthetically active radiation (PAR) (Fig. 2a). The average rainfall from May through October is much lower than other months, with July and August being the driest. Radiation reaches its lowest value in May, starts increasing from June and stays at a high level over July – October. The seasonal cycle of clouds (COT) is similar to rainfall, with low values in the dry season (Fig. 2b). In contrast, the aerosol concentration (AOD) is much higher during the dry season (August–October) mainly due to large-scale biomass burning activities (Artaxo *et al.*, 2013).

Figure 2c shows the seasonal cycle of TWS, LST and VPD over southern Amazonia. The TWS reaches its peak value in April and starts to decline from May onwards. After hitting its lowest value in October (referred to as TWS_{MIN}), it increases again with increased rainfall and decreased radiation. Both VPD and LST increase at the start of the dry season and reach the highest values in August and October, respectively, which are referred to as VPD_{MAX} and LST_{MAX}.

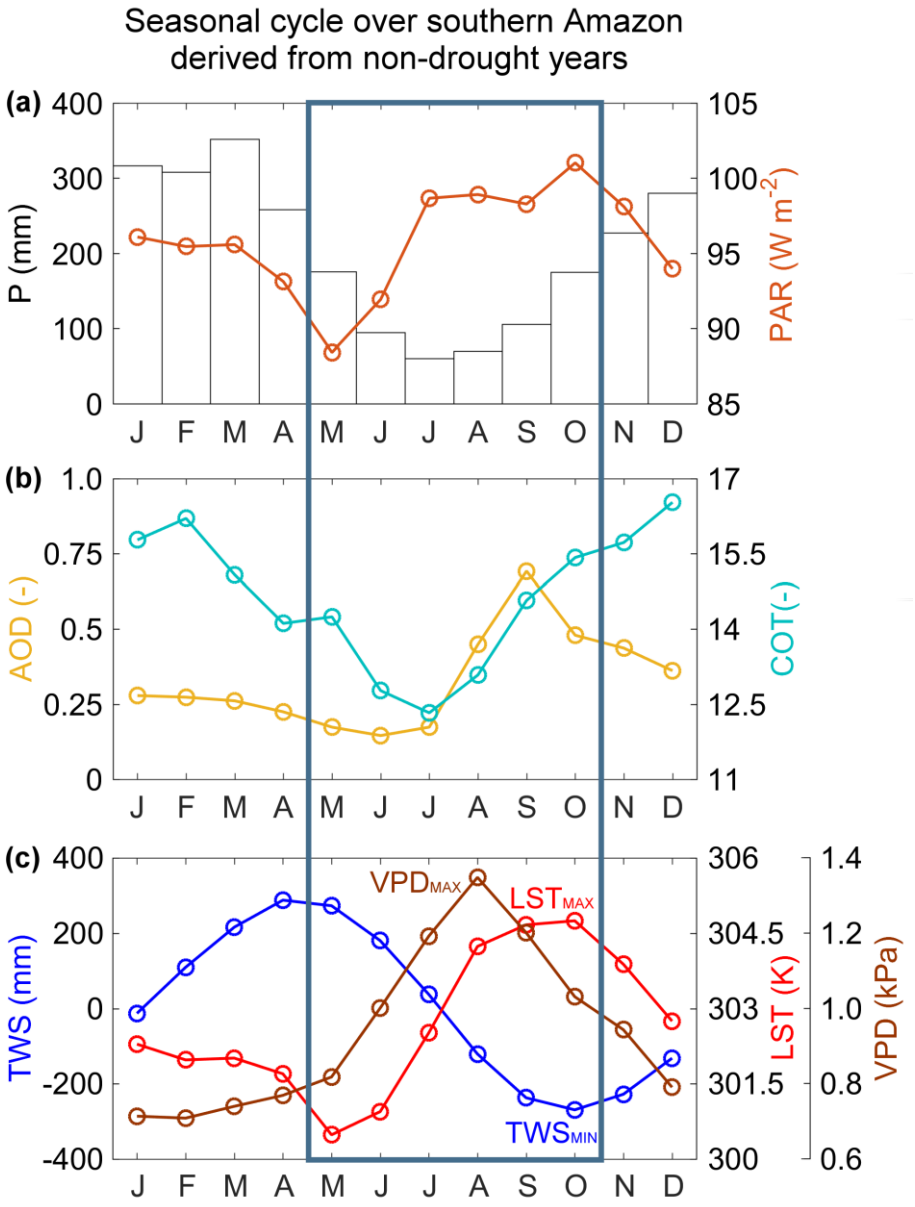

290

291 **Fig 2.** Hydrometeorological dynamics over southern Amazonia during non-drought years.

292 Seasonal cycles of rainfall (P, mm month^{-1}), photosynthetically active radiation (PAR, W

293 m^{-2}), aerosol optical depth (AOD), cloud optical thickness (COT), terrestrial water storage

294 (TWS, mm), land surface temperature (LST, K) and vapor pressure deficit (VPD, kPa) over

295 the intact forest region in southern Amazonia during non-drought years (i.e., averaged over

296 2003–2010, excluding 2005 and 2010). The anomalies in 2005 and 2010 will be examined in

297 detail over the extended dry season (May–October) that is outlined by the blue box.

298 Given the difference in the timing of the rainfall anomalies between 2005 and 2010, we
299 separately considered hydrometeorological conditions during the onset of droughts in the
300 wet-to-dry season (May–July) and during the peak of droughts in the dry season
301 (August–October) (Fig. 3). Strong rainfall anomalies were observed in the wet-to-dry season
302 in 2005, whereas the rainfall in 2010 was only slightly below average (Fig. 3a). By contrast,
303 rainfall deficits were observed in the dry season in both years, but much stronger in 2010.

304 In both years, radiation was generally above average during the wet-to-dry season and below
305 average during the dry season (Fig. 3b), but the magnitudes of anomalies differed between
306 these two years. Radiation was above average in May and June of both years corresponding to
307 below-average cloudiness. While radiation was still above average in July 2005, increased
308 cloud cover reduced radiation to below average in July 2010. Conversely, greater aerosol
309 loads and cloudiness in August–September 2005 caused a stronger negative radiation anomaly
310 when compared to 2010 (Fig. 3c, d). Negative rainfall and high-level radiation caused strong
311 anomalies in TWS, LST and VPD (Fig. 3e, f, g). These variables exceeded their ranges of
312 non-drought years, with stronger magnitudes in 2010.

313 Spatially, significant negative anomalies in rainfall were primarily observed over
314 southwestern Amazonia during both wet-to-dry and dry seasons in 2005, and over entire
315 southern Amazonia during the dry season in 2010 (Fig. 4a, b, c, d). Spatial patterns of positive
316 radiation anomalies agreed well with negative rainfall anomalies during the wet-to-dry season
317 in both years (Fig. 4e, f). The overall positive radiation anomalies can be attributed to strong
318 positive anomalies in direct PAR and weak negative anomalies in diffuse PAR (Fig. S2) as a
319 consequence of reduced cloud cover and/or aerosol loads. On the other hand, strong negative

anomalies in radiation related to high aerosol content were observed in the dry season of both events, with greater magnitudes and spatial coverage in 2005 (Fig. 4g, h).

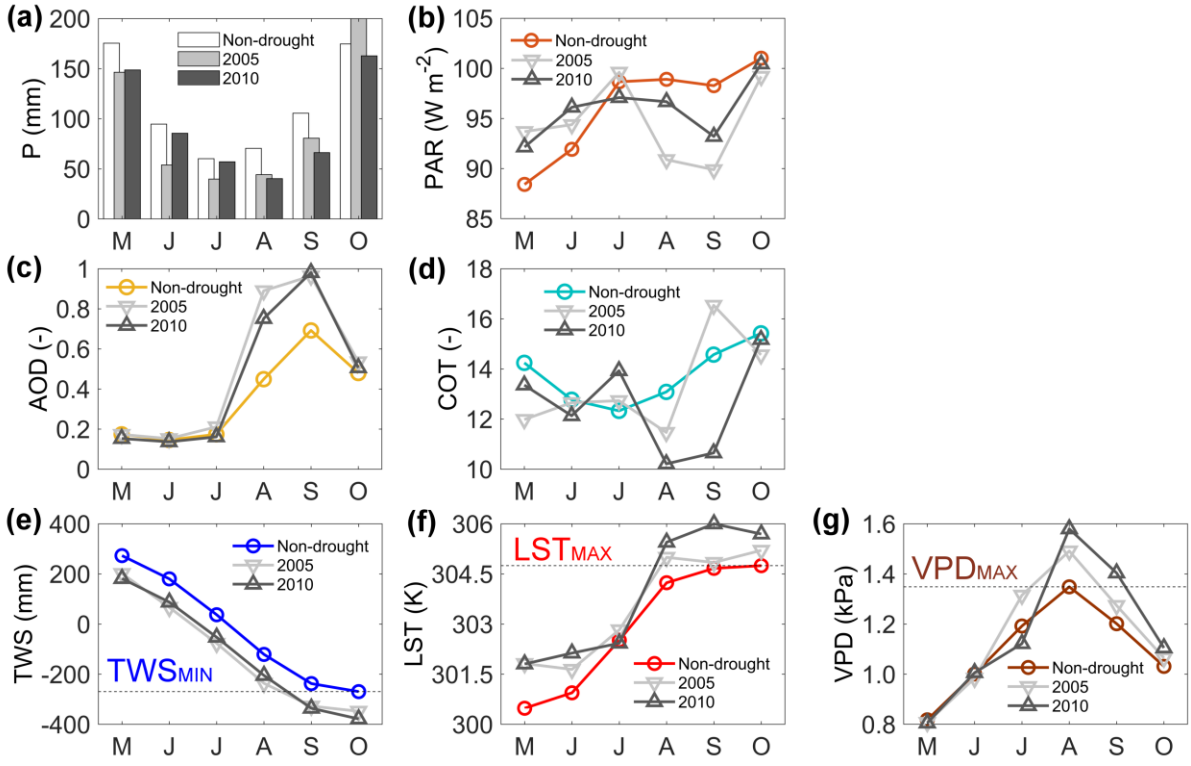

Fig 3. Hydrometeorological anomalies over southern Amazonia in the 2005 and 2010 droughts. Time series of monthly average (a) rainfall (P), (b) photosynthetically active radiation (PAR), (c) aerosol optical depth (AOD), (d) cloud optical thickness (COT), (e) terrestrial water storage (TWS), (f) land surface temperature (LST) and (g) vapor pressure deficit (VPD) over southern Amazonia from May through October in 2005 and 2010 in comparison with non-drought years, respectively.

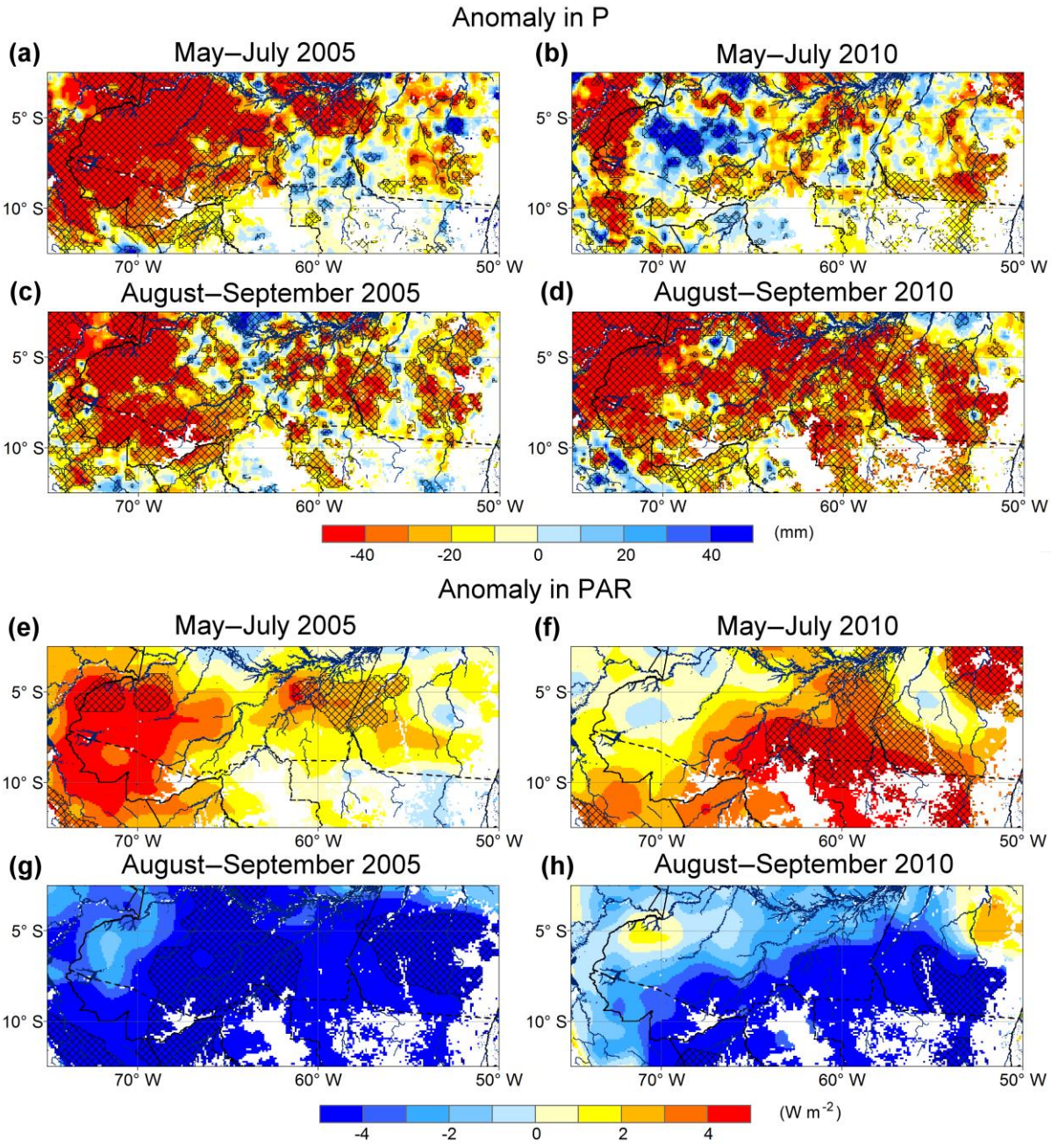

Fig 4. Anomalies in rainfall (P, mm) and photosynthetically active radiation (PAR, W m^{-2}) for the onset of drought during the wet-to-dry season (May–July) and the peak of drought during the dry season (August–September) of 2005 and 2010. Anomalies represent the departure from the average of non-drought years. The areas with statistically significant anomalies based on non-parametric Wilcoxon signed rank test (p<0.05) are hatched.

3.2 Vegetation response during the onset of droughts

Figure 5 shows the standardized anomalies in VOD, LAI and EVI during the onset of droughts in the wet-to-dry season (May–July) of 2005 and 2010. As the concentration of atmospheric aerosols was low in these three months (Fig. 3c), the optical vegetation information (i.e., LAI and EVI) can be expected to be reliable. These three vegetation variables represent different properties of the forest canopy (i.e., VOD for canopy water content, LAI for leaf area and EVI for canopy greenness), but all show large-scale positive anomalies during the onset of both droughts. Table 2 lists the percentage of southern Amazonia with VOD, LAI and EVI anomalies of different magnitudes during the onset of droughts in 2005 and 2010. The median anomalies in VOD, LAI and EVI were all positive in both years, but their magnitudes differed significantly (p<0.05) and were stronger overall in 2005 than in 2010.

These positive anomalies in VOD, LAI and EVI in both years, as well as their differences, seem related to the hydrometeorological conditions. In 2005, strong rainfall deficits during the onset of droughts were associated with above-average radiation (Fig. 3a, b), resulting in a positive anomaly in both VPD and canopy temperature, and a negative anomaly in terrestrial water storage (Fig. 3e, f, g). However, they did not exceed the VPD_{MAX}, LST_{MAX} and TWS_{MIN} observed during non-drought years (Fig. 6), suggesting (1) that there was a higher atmospheric moisture demand but still sufficient soil water supply remained available for photosynthesis and growth and (2) that heat and water stress in the top of the canopy were within the typical dry season ranges. In addition, the diurnal VOD signals between drought and non-drought years were compared following the approach in Konings and Gentine (2017).

The results suggest that there is little evidence for stomatal closure during the onset of droughts over southern Amazonia in May–July 2005 and 2010 compared to the non-drought years (Fig. S3).

Below-average rainfall and above-average radiation during the onset of droughts appears to be equivalent to an early arrival of normal dry season, during which enhanced leaf development and ecosystem photosynthesis in Amazonia are observed according to field observations (Wu *et al.*, 2016). The strong positive anomalies in VOD, LAI, and EVI, occurred during these three months, are therefore consistent with the expected increase in leaf production under sufficient soil water supply (Brando *et al.*, 2010, Nepstad *et al.*, 1994). The enhanced canopy growth in May–July 2005 was much stronger than 2010, which is very likely due to the greater positive anomalies in radiation in 2005 (as shown Fig. 3 and 4). Furthermore, the distribution of standardized anomalies in VOD during the onset of droughts was compared with that at the end of 2004 and 2009. The results suggest that the positive anomalies in VOD during the onset of both droughts are likely caused by the unusual hydrometeorological conditions in the drought years, and not a delayed response to the previous year (Fig. S4).

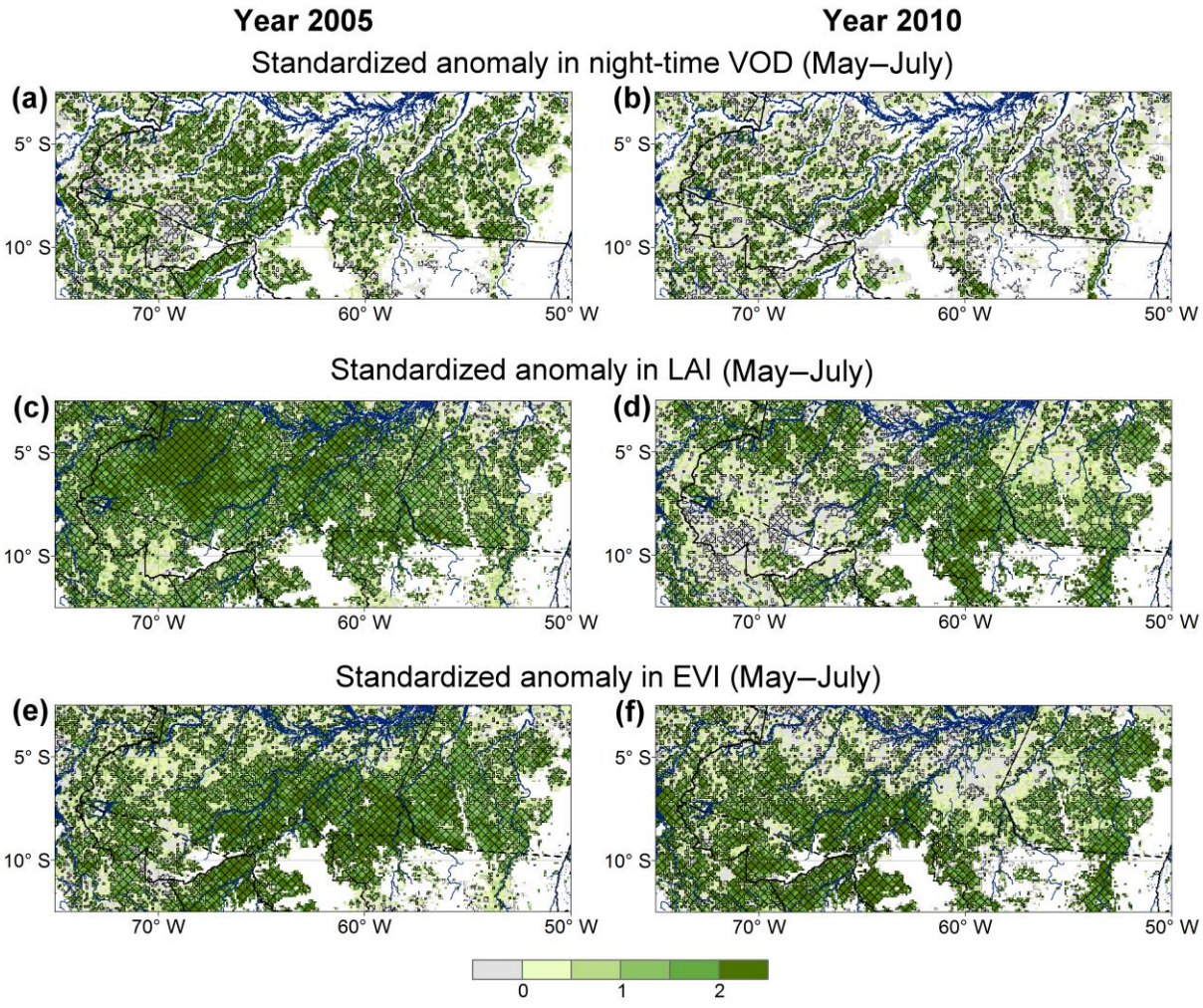

374

375 **Fig 5.** Standardized anomalies in vegetation indicators during the onset of droughts

376 (May–July) in 2005 and 2010. Units represent the number of standard deviations as a

377 departure from the average of non-drought years in (a and b) night-time vegetation optical

378 depth (VOD), (c and d) leaf area index (LAI), and (e and f) enhanced vegetation index (EVI).

379 Areas with statistically significant anomalies based on the non-parametric Wilcoxon signed

380 rank test ($p<0.05$) are hatched.

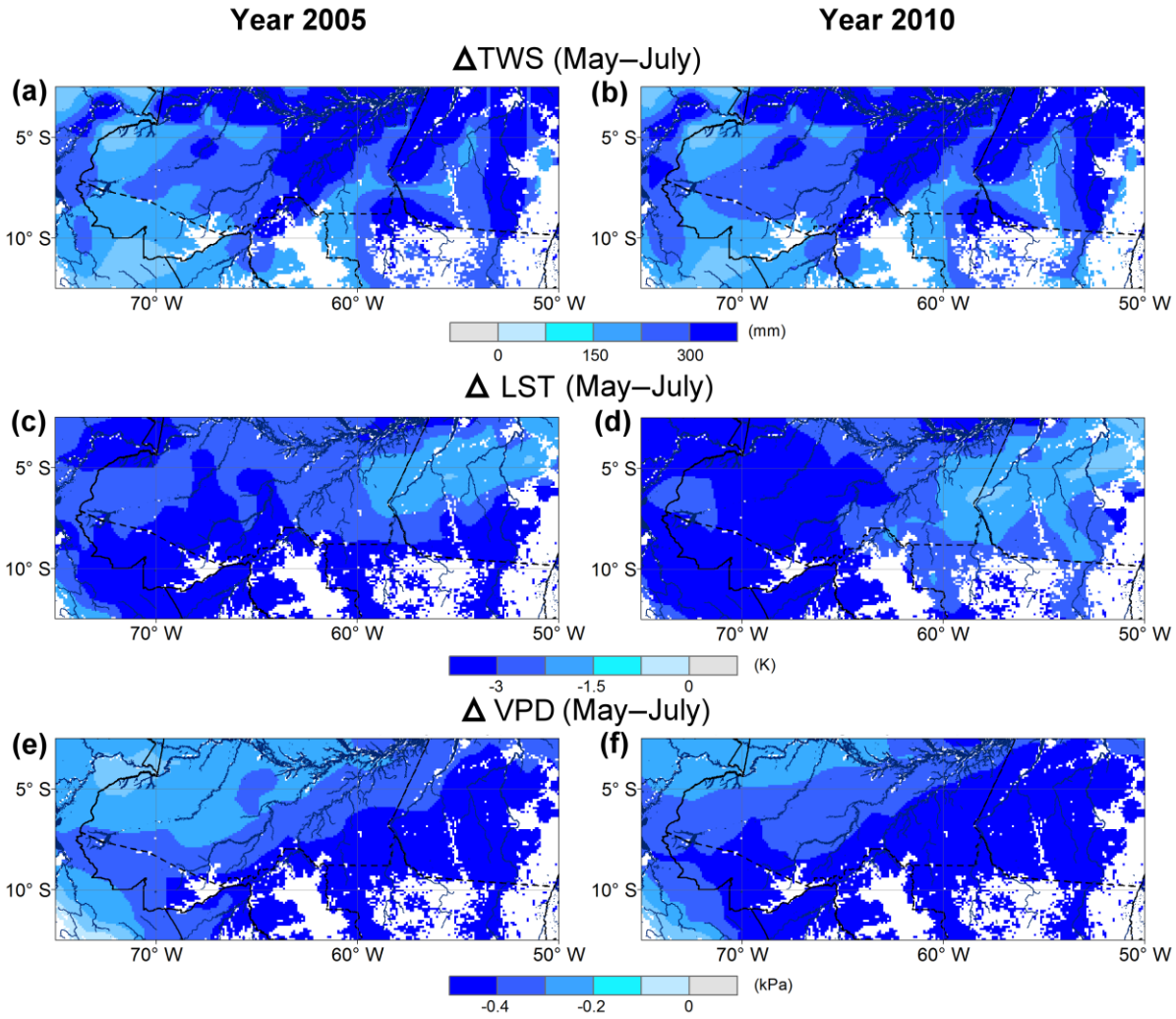

381

382 **Fig 6.** (a and b) Mean TWS over May–July minus TWS_{MIN} during the non-drought years for
383 each grid cell (ΔTWS). (c and d) Mean LST over May–July minus LST_{MAX} during the
384 non-drought years (ΔLST). (e and f) Mean VPD over May–July minus VPD_{MAX} during the
385 non-drought years (ΔVPD).

386

387

388

389

390 **Table 2.** Percentage of southern Amazonia corresponding to different anomaly magnitudes for

391 VOD, LAI and EVI during May – July in 2005 and 2010.

May – July	<-2 SD[1]	-2 to -1 SD	-1 to 1 SD	1 to 2 SD	>2 SD	Total	Median anomaly ± SD	Significantly different ($p<0.05$)
VOD								
2005	0.9%	3.9%	58.2%	25.6%	11.3%	100%	0.77 ± 1.09	Yes
2010	2.6%	9.1%	67.8%	14.6%	5.9%	100%	0.21 ± 1.09	
LAI								
2005	0.1%	0.3%	29.3%	44.1%	26.3%	100%	1.39 ± 1.12	Yes
2010	0.9%	3.9%	51.2%	31.8%	12.1%	100%	0.86 ± 1.15	
EVI								
2005	0.2%	0.9%	32.8%	34.9%	31.1%	100%	1.43 ± 1.32	Yes
2010	0.4%	1.4%	40.1%	32.1%	25.9%	100%	1.21 ± 1.41	

392 [1] SD: standard deviation

393 ***3.3 Vegetation response during the peak of droughts***

394 Due to the presence of extremely high atmospheric aerosols during the peak of 2005 and 2010

395 droughts (Fig. 3c), the accuracy of optical observations is expected to be adversely affected.

396 Therefore we excluded LAI and EVI from this section and only focused on VOD. Anomalies

397 in canopy water content (represented by VOD) during the peak of droughts (August–October)

398 of both drought years are presented in Fig. 7. Significantly negative anomalies in VOD were

399 found primarily over southwestern Amazonia in 2005 (Fig. 7a). The spatial pattern of VOD

400 anomalies agrees well with the findings of Saatchi *et al.* (2012) in which the radar backscatter

401 from QSCAT was used to characterize the anomalies in canopy structure and moisture in 2005.

In the event of 2010, significantly negative anomalies in VOD were more widespread, covering the central and eastern parts of southern Amazonia (Fig. 7b). Similar spatial patterns of negative VOD anomalies were also found in the day-time retrievals despite higher uncertainties (Fig. S5).

Table 3 summarizes the fractions of southern Amazonia (%) for different magnitudes of VOD anomalies during the peak of droughts (August–October) of both events. When all grid cells over southern Amazonia are considered, 14.3% and 14.8% of the area showed anomalies more than two standard deviations below the average for non-drought years (i.e., <-2 SD) in 2005 and 2010, respectively. The median (±SD) standardized anomaly is -0.51 (±2.07) and -0.56 (±1.48), respectively for 2005 and 2010; their difference is not statistically significant (i.e., $p>0.05$) based on non-parametric Wilcoxon signed rank test. When only taking account the grid cells with strong negative anomalies (i.e., less than two standard deviations), the mean standardized anomaly is -2.78 and -2.65 for 2005 and 2010, respectively; this difference is statistically significant ($p<0.05$).

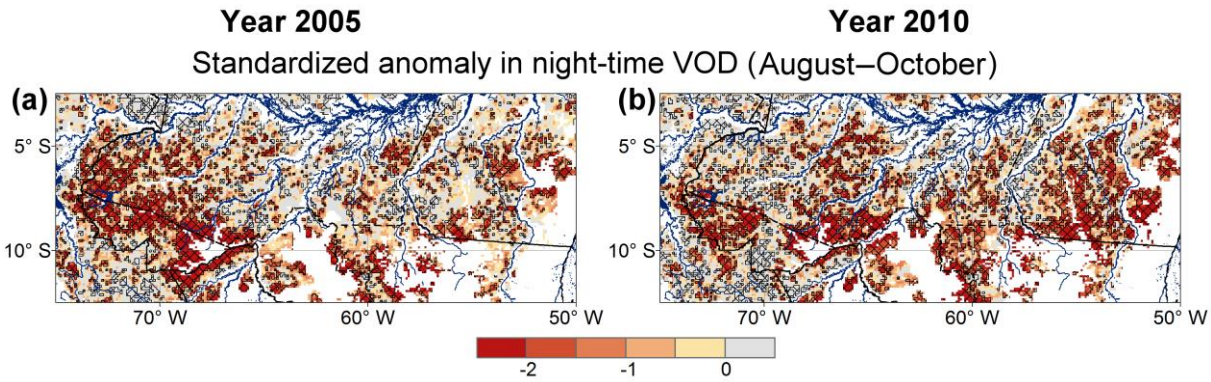

417

418 **Fig 7.** Standardized anomalies in night-time VOD during the peak of droughts

419 (August–October) in 2005 and 2010. Units represent the number of standard deviations as a

420 departure from the average of non-drought years. Areas with statistically significant

421 anomalies based on non-parametric Wilcoxon signed rank test (p<0.05) are hatched.

422 **Table 3.** Percentage of southern Amazonia corresponding to different anomaly magnitudes for

423 VOD during August–October in 2005 and 2010.

For all grid cells over southern Amazonia								
August – October	<-2 SD	-2 to -1 SD	-1 to 1 SD	1 to 2 SD	>2 SD	Total	Median anomaly ± SD	Significantly different (p<0.05)
2005	14.3%	19.7%	56.3%	6.9%	2.8%	100%	-0.51 ± 2.07	No
2010	14.8%	21.6%	51.0%	8.7%	3.9%	100%	-0.56 ± 1.55	
For the grid cells with "<-2 SD" anomaly								
August – October	<-6 SD	-6 to -5 SD	-5 to -4 SD	-4 to -3 SD	-3 to -2 SD	Total	Median anomaly ± SD	Significantly different (p<0.05)
2005	0.7%	0.6%	1.3%	3.3%	8.4%	14.3%	-2.78 ± 1.36	Yes
2010	0.3%	0.4%	1.1%	3.2%	9.8%	14.8%	-2.65 ± 1.02	

424

425 Meanwhile, terrestrial water storage was well below TWS_{MIN}, and canopy temperatures and
426 vapor pressure deficit were above LST_{MAX} and VPD_{MAX}, respectively (Fig. 8a-f). Similar
427 spatiotemporal patterns in VPD were found when using ERA-interim data (see Fig. S6),
428 further supporting the AIRS-based VPD estimates. These strong anomalies were observed
429 over large parts of southwestern Amazonia in 2005 and over the central and eastern parts of
430 southern Amazonia in 2010. While the magnitude and spatial coverage of negative TWS
431 anomalies were greater in 2010 (Fig. 8a, b), the soil moisture stress based on the magnitude
432 and duration of rainfall deficit was much stronger in 2005 (Fig. 8g, h). The spatial agreements
433 between negative VOD anomalies and hydrometeorological anomalies strongly suggest that
434 below-average canopy water content resulted from the combined effects of severe water stress
435 and heat stress, which agrees with the findings of Toomey *et al.* (2011). They found that
436 jointly considering heat and moisture stress can better explain the reduction of aboveground
437 living biomass observed by the ground RAINFOR network.

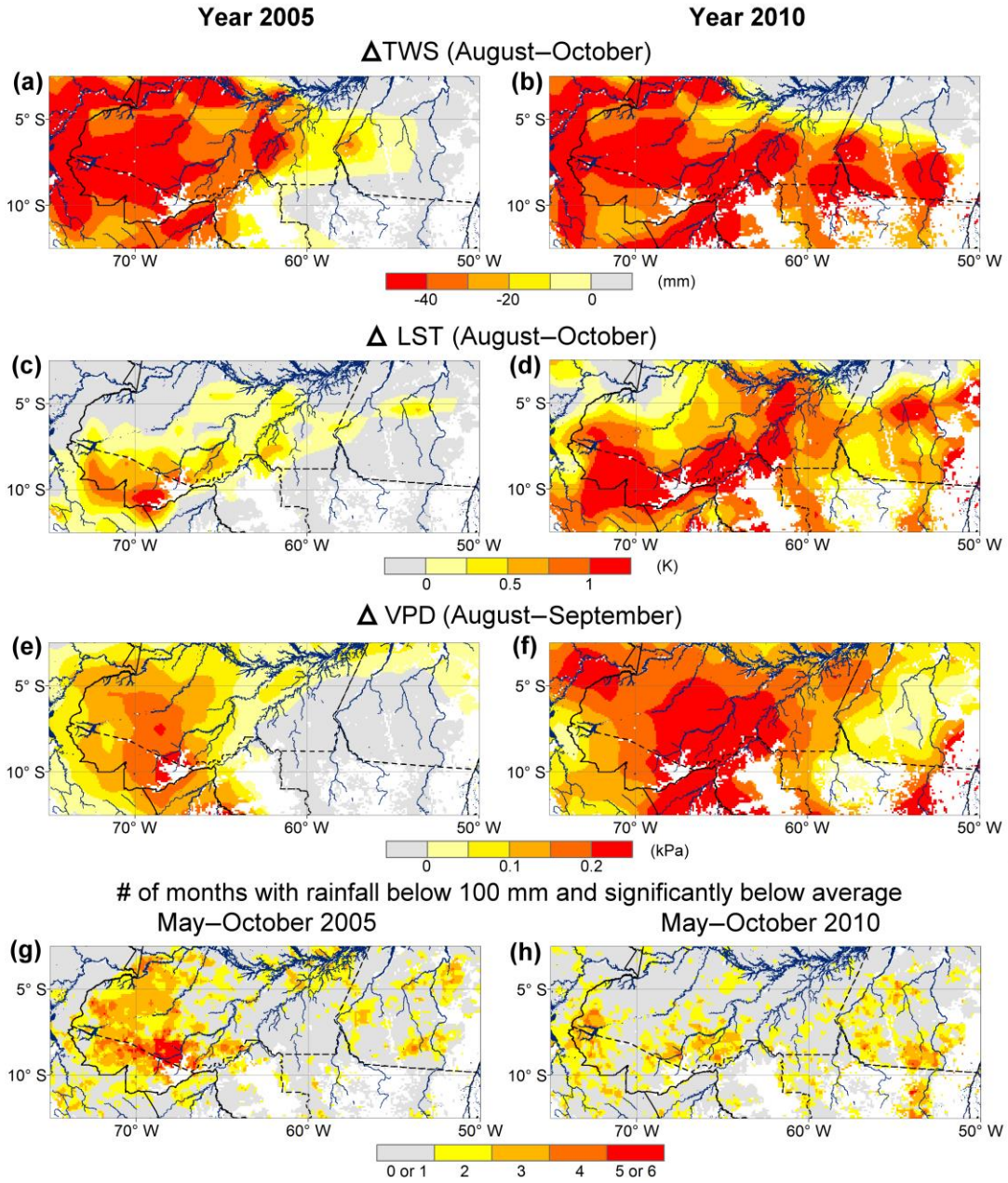

438

439 **Fig 8.** (a and b) Mean TWS over August–October minus TWS_{MIN} during the non-drought

440 years for each grid cell (ΔTWS). (c and d) Mean LST over August–October minus LST_{MAX}

441 during the non-drought years (ΔLST). (e and f) Mean VPD over August–September minus

442 VPD_{MAX} during the non-drought years (ΔVPD). (g and h) Total number of months with

443 monthly rainfall below 100 mm and significantly below average of non-drought years,

444 between May and October in 2005 and 2010 respectively for each grid cell.

3.4 Possible causes for the difference in response to 2005 and 2010 drought events

During the 2005 and 2010 droughts, significantly negative anomalies in canopy water content, represented by VOD, were found primarily over southwestern Amazonia in 2005, while negative VOD anomalies were located in central and eastern parts of southern Amazonia in 2010. The total areas with negative VOD anomalies greater than two standard deviations were similar during the two droughts (i.e., 14.3% and 14.8%, respectively). When only considering the grid cells with more than two standard deviations below the average, the 2005 drought showed a significantly more severe decline in canopy water content. This qualitatively agrees with field observations that suggest the reduction in carbon uptake was stronger in 2005 than 2010 (Feldpausch *et al.*, 2016). Interestingly, Feldpausch *et al.* (2016) also found that reduced carbon uptake was primarily caused by increased tree mortality in 2005, but by a combination of high mortality and slow tree growth in 2010. During both droughts, reduced carbon uptake (i.e., the combined effect of tree mortality and slow tree growth) was related to the strength of moisture deficit. But in 2010, there was no clear relationship between increased tree mortality and water deficit anomaly (Feldpausch *et al.*, 2016).

Our findings help to scale up and explain these field observations. Firstly, the duration of soil moisture depletion (i.e., monthly rainfall below 100 mm and significantly below average of non-drought years) was much greater in 2005 than 2010 (Fig. 8g, h). A large part of southwestern Amazonia experienced three or more months of soil moisture depletion in 2005, whereas only a few small areas did in 2010. Moreover, enhanced canopy growth during the onset of 2005 drought in the wet-to-dry season (May–July) would accelerate soil moisture depletion. Significant negative VOD anomalies were found in these regions with three or

more months of soil moisture depletion in both droughts, regardless of the magnitude of temperature and VPD anomalies. This suggests that soil moisture stress in these regions may have exceeded the tolerance limit of the rainforest, resulting in declines in canopy water content and presumably increased tree mortality.

Secondly, from the onset to the peak of drought in 2010, most of southern Amazonia experienced only one month of soil moisture depletion (Fig. 8h), mainly in August and September. This indicates that a soil water deficit likely occurred in the shallow soil, rather than at greater depth. Then high canopy temperature and atmospheric moisture demand during August–September 2010 appeared to have resulted primarily from a concurrent strong rainfall deficit and high radiation flux, rather than insufficient soil water supply alone. The high temperatures and atmospheric moisture demand can cause near-instantaneous declines in carbon assimilation and slow tree growth (Doughty & Goulden, 2008, Toomey *et al.*, 2011), but may not have been severe enough to cause large-scale mortality.

The above findings are supported by the two partial throughfall exclusion experiments (TFEs) over eastern Amazonia (Brando *et al.*, 2008, da Costa *et al.*, 2010, Rowland *et al.*, 2015), in which a fraction of the throughfall was prevented from infiltrating into the soil. In one experiment, throughfall was reduced continuously for several years, while in the other experiment only wet season throughfall was reduced. Soil moisture, tree mortality and wood volume were recorded in both experiments and compared with nearby control plots. Both experiments showed that soil water in the TFE declined with time, but tree mortality was similar to that in the control plots during the first 2-3 years. When soil water in the TFE plots fell below an apparent threshold after this period, tree mortality in the TFE plots became

489 significantly higher, particularly among tall trees, than in the control plots. The elevated
490 mortality was most likely due to the strongly reduced soil water potential and vulnearability
491 of tall trees to xylem cavitation (Rowland et al. 2015). However, above-ground wood
492 production was already reduced in TFE plots from the second year of throughfall exclusion.
493 Qualitatively these processes support our satellite-based analysis presented here, although the
494 multiple TFE experiments cannot be compared directly with the natural seasonal droughts in
495 2005 and 2010, as the experiments only reduced soil water without increased surface
496 temperature or atmospheric moisture demand. During the 2005 drought, the accelerated soil
497 moisture depletion may have reduced soil moisture levels below the critical threshold and
498 increase tree mortality. This may be particularly expected in southwestern Amazonia where
499 trees are known to have relatively shallow root systems (Quesada *et al.*, 2011, Quesada *et al.*,
500 2010).

501 Our findings help to explain the different rainforest responses in 2005 and 2010 as also
502 observed in the field, but our analysis has limitations of its own. For example, VOD is a
503 dimensionless variable that captures the relative dynamics of canopy water content in
504 Amazonian rainforest as illustrated in this study, but the quantitative relationship between
505 VOD and canopy water content for Amazonian rainforest is not yet known, and we could not
506 quantify the absolute anomalies of canopy water content during the 2005 and 2010 droughts.

507 **4. Conclusions**

508 In summary, our study convincingly identified two stages the evolution of the Amazonian
509 droughts of 2005 and 2010. During the onset of droughts in the wet-to-dry season (May–July),
510 below-average rainfall and above-average radiation led to an early arrival of normal dry

season with enhanced leaf development and ecosystem photosynthesis while there was sufficient soil water. During the peak of droughts in the dry reason (August–October), the drought intensification negatively impacted forest growth and canopy senescence occurred under severe water and heat stress. The magnitude and timing of enhanced canopy growth and subsequent senescence were different for the two droughts. This was primarily caused by the contrasting spatiotemporal evolution in rainfall, radiation and atmospheric moisture demand. Aerosols from biomass burning in the dry season reduced incoming radiation in both years (Artaxo *et al.*, 2013, Ten Hoeve *et al.*, 2012). Without this reduction in radiation, water and heat stress over the intact forests of southern Amazonia might have been even more severe. To better understand the future of the Amazonian rainforests in response to climate change, the interactions between these natural and anthropogenic factors need to be better understood and represented in climate and vegetation models. As demonstrated here, interrogating independent but complementary satellite and field observations can help develop a better understanding of this complex and critical biome.

Acknowledgements

YYL is a recipient of Thousand Talents Plan for Young Outstanding Scientists, and acknowledges the financial support from the Nanjing University Information Science and Technology (NUIST) startup grant (2243141701020). DGM acknowledges support from the European Research Council (ERC) under grant agreement 715254 (DRY–2–DRY), and the Belgian Science Policy Office (BELSPO) in the framework of the STEREO III programme projects SAT-EX (SR/00/306) and STR3S (SR/02/329). MFM is supported by the King Abdullah University of Science and Technology. PG acknowledges DOE GoAmazon grant

533 DE-SC0011094. All authors would like to thank Alexei Lyapustin and Yujie Wang for
534 providing the EVI based on MAIAC algorithm (Collection 6). GRACE land data were
535 processed by Sean Swenson, supported by the NASA MEaSUREs Program and available at
536 http://grace.jpl.nasa.gov. The authors declare no conflict of interest.

537 **References**

538 Andela, N., Liu, Y.Y., van Dijk, A.I.J.M., de Jeu, R.A.M., & McVicar, T.R. (2013). Global
539 changes in dryland vegetation dynamics (1988-2008) assessed by satellite remote
540 sensing: comparing a new passive microwave vegetation density record with reflective
541 greenness data. *Biogeosciences, 10,* 6657-6676.

542 Aragao, L.E.O.C., Malhi, Y., Roman-Cuesta, R.M., Saatchi, S., Anderson, L.O., &
543 Shimabukuro, Y.E. (2007). Spatial patterns and fire response of recent Amazonian
544 droughts. *Geophysical Research Letters, 34,* L07701, doi:10.1029/2006GL028946.

545 Artaxo, P., Rizzo, L.V., Brito, J.F., Barbosa, H.M.J., Arana, A., Sena, E.T., et al. (2013).
546 Atmospheric aerosols in Amazonia and land use change: from natural biogenic to
547 biomass burning conditions. *Faraday Discussions, 165,* 203-235.

548 Atkinson, P.M., Dash, J., & Jeganathan, C. (2011). Amazon vegetation greenness as measured
549 by satellite sensors over the last decade. *Geophysical Research Letters, 38,* L19105,
550 doi:10.1029/2011GL049118.

551 Bi, J., Myneni, R., Lyapustin, A., Wang, Y., Park, T., Chi, C., et al. (2016). Amazon Forests'
552 Response to Droughts: A Perspective from the MAIAC Product. *Remote Sensing, 8,* 356,
553 doi:10.3390/rs8040356.

554 Brando, P.M., Goetz, S.J., Baccini, A., Nepstad, D.C., Beck, P.S.A., & Christman, M.C.
555 (2010). Seasonal and interannual variability of climate and vegetation indices across the
556 Amazon. *Proceedings of the National Academy of Sciences of the United States of*
557 *America, 107,* 14685-14690.

558 Brando, P.M., Nepstad, D.C., Davidson, E.A., Trumbore, S.E., Ray, D., & Camargo, P. (2008).
559 Drought effects on litterfall, wood production and belowground carbon cycling in an
560 Amazon forest: results of a throughfall reduction experiment. *Philosophical Transactions*
561 *of the Royal Society B-Biological Sciences, 363,* 1839-1848.

562 da Costa, A.C.L., Galbraith, D., Almeida, S., Portela, B.T.T., da Costa, M., Silva, J.D., et al.
563 (2010). Effect of 7 yr of experimental drought on vegetation dynamics and biomass
564 storage of an eastern Amazonian rainforest. *New Phytologist, 187,* 579-591.

565 de Jeu, R.A.M., Holmes, T.R.H., Parinussa, R.M., & Owe, M. (2014). A spatially coherent
566 global soil moisture product with improved temporal resolution. *Journal of Hydrology,*
567 *516,* 284-296.

568 Doughty, C.E., & Goulden, M.L. (2008). Seasonal patterns of tropical forest leaf area index
569 and CO_2 exchange. *Journal of Geophysical Research: Biogeosciences, 113,* G00B06,
570 doi:10.1029/2007JG000590.

571 Doughty, C.E., Metcalfe, D.B., Girardin, C.A.J., Amezquita, F.F., Cabrera, D.G., Huasco,
572 W.H., et al. (2015). Drought impact on forest carbon dynamics and fluxes in Amazonia.
573 *Nature, 519,* 78-82.

574 Feldpausch, T.R., Phillips, O.L., Brienen, R.J.W., Gloor, E., Lloyd, J., Lopez-Gonzalez, G., et

al. (2016). Amazon forest response to repeated droughts. *Global Biogeochemical Cycles, 30,* 964-982.

Fisher, R.A., Williams, M., Do Vale, R.L., Da Costa, A.L., & Meir, P. (2006). Evidence from Amazonian forests is consistent with isohydric control of leaf water potential. *Plant, Cell and Environment, 29,* 151-165.

Fisher, R.A., Williams, M., da Costa, A.L., Almeida, S., Meir, P., et al. (2007). The response of an Eastern Amazonian rain forest to drought stress: results and modelling analyses from a throughfall exclusion experiment. *Global Change Biology 13,* 2361–2378.

Friedl, M.A., Sulla-Menashe, D., Tan, B., Schneider, A., Ramankutty, N., Sibley, A., et al. (2010). MODIS Collection 5 global land cover: Algorithm refinements and characterization of new datasets. *Remote Sensing of Environment, 114,* 168-182.

Gatti, L.V., Gloor, M., Miller, J.B., Doughty, C.E., Malhi, Y., Domingues, L.G., et al. (2014). Drought sensitivity of Amazonian carbon balance revealed by atmospheric measurements. *Nature, 506,* 76-80.

Gibbons, J.D., & Chakraborti, S. (2011). Nonparametric Statistical Inference. (5th Revised Edition ed.). Boca Raton, FL, United States: Taylor & Francis Ltd.

Guan, K., Pan, M., Li, H., Wolf, A., Wu, J., Medvigy, D., et al. (2015). Photosynthetic seasonality of global tropical forests constrained by hydroclimate. *Nature Geoscience, 8,* 284-289.

Guglielmetti, M., Schwank, M., Matzler, C., Oberdorster, C., Vanderborght, J., & Fluhler, H. (2007). Measured microwave radiative transfer properties of a deciduous forest canopy.

596 *Remote Sensing of Environment, 109,* 523-532.

597 Huffman, G.J., Adler, R.F., Bolvin, D.T., Gu, G.J., Nelkin, E.J., Bowman, K.P., et al. (2007).
598 The TRMM multisatellite precipitation analysis (TMPA): Quasi-global, multiyear,
599 combined-sensor precipitation estimates at fine scales. *Journal of Hydrometeorology, 8,*
600 38-55.

601 Jackson, T.J., & Schmugge, T.J. (1991). Vegetation Effects on the Microwave Emission of
602 Soils. *Remote Sensing of Environment, 36,* 203-212.

603 Jarvis P G. (1976). The interpretation of the variations in leaf water potential and stomatal
604 conductance found in canopies in the field. *Philosophical Transactions of the Royal*
605 *Society of London. Biological Sciences: Series B, 273,* 593–610.

606 Jiménez-Muñoz, J. C., Mattar, C., Barichivich, J., Santamaría-Artigas, A., Takahashi, K.,
607 Malhi, Y., et al. (2016). Record-breaking warming and extreme drought in the Amazon
608 rainforest during the course of El Niño 2015–2016. *Scientific Reports, 6,* 33130.

609 Jones, M.O., Jones, L.A., Kimball, J.S., & McDonald, K.C. (2011). Satellite passive
610 microwave remote sensing for monitoring global land surface phenology. *Remote*
611 *Sensing of Environment, 115,* 1102-1114.

612 Jones, M.O., Kimball, J.S., & Jones, L.A. (2013). Satellite microwave detection of boreal
613 forest recovery from the extreme 2004 wildfires in Alaska and Canada. *Global Change*
614 *Biology, 19,* 3111-3122.

615 Kerr, Y.H., & Njoku, E.G. (1990). A semiempirical model for interpreting microwave
616 emission from semiarid land surfaces as seen from space. *IEEE Transactions on*

Geoscience and Remote Sensing, 28, 384-393.

Kirdyashev, K.P., Chukhlantsev, A.A., & Shutko, A.M. (1979). Microwave Radiation of the Earth's surface in the presence of a vegetation cover. *Radio Engineering & Electronic Physics, 24,* 37-44.

Konings, A. G., & Gentine. P. (2017). Global variations in ecosystem-scale isohydricity. *Global change biology, 23,* 891-905.

Landerer, F.W., & Swenson, S.C. (2012). Accuracy of scaled GRACE terrestrial water storage estimates. *Water Resources Research, 48,* W04531, doi: 10.1029/2011wr011453.

Lee, J. E., Frankenberg, C., van der Tol, C., Berry, J.A., Guanter, L., Boyce, C.K., et al. (2013). Forest productivity and water stress in Amazonia: observations from GOSAT chlorophyll fluorescence. *Proceedings of the Royal Society B: Biological Sciences, 280,* doi: 10.1098/rspb.2013.0171.

Leuning R. (1995). A critical appraisal of a combined stomatal- photosynthesis model for C_3 plants. *Plant, Cell and Environment, 18,* 339−355.

Lewis, S.L., Brando, P.M., Phillips, O.L., van der Heijden, G.M.F., & Nepstad, D. (2011). The 2010 Amazon Drought. *Science, 331,* 554.

Liu, Y.Y., van Dijk, A.I.J.M., de Jeu, R.A.M., Canadell, J.G., McCabe, M.F., Evans, J.P., et al. (2015). Recent reversal in loss of global terrestrial biomass. *Nature Climate Change, 5,* 470-474.

Liu, Y.Y., van Dijk, A.I.J.M., McCabe, M.F., Evans, J.P., & de Jeu, R.A.M. (2013). Global vegetation biomass change (1988–2008) and attribution to environmental and human

drivers. *Global Ecology and Biogeography, 22*, 692-705.

Lyapustin, A., Martonchik, J., Wang, Y., Laszlo, I., & Korkin, S. (2011a). Multiangle implementation of atmospheric correction (MAIAC): 1. Radiative transfer basis and look-up tables. *Journal of Geophysical Research: Atmospheres, 116,* D03210, doi: 10.1029/2010JD014985.

Lyapustin, A., Wang, Y., Laszlo, I., Kahn, R., Korkin, S., Remer, L., et al. (2011b). Multiangle implementation of atmospheric correction (MAIAC): 2. Aerosol algorithm. *Journal of Geophysical Research: Atmospheres, 116,* D03211, doi: 10.1029/2010JD014986.

Lyapustin, A.I., Wang, Y., Laszlo, I., Hilker, T., G. Hall, F., Sellers, P.J., et al. (2012). Multi-angle implementation of atmospheric correction for MODIS (MAIAC): 3. Atmospheric correction. *Remote Sensing of Environment, 127,* 385-393.

Marengo, J.A., & Espinoza, J.C. (2016). Extreme seasonal droughts and floods in Amazonia: causes, trends and impacts. *International Journal of Climatology, 36,* 1033-1050.

Meesters, A.G.C.A., De Jeu, R.A.M., & Owe, M. (2005). Analytical derivation of the vegetation optical depth from the microwave polarization difference index. *IEEE Geoscience and Remote Sensing Letters, 2,* 121-123.

Morton, D.C., Nagol, J., Carabajal, C.C., Rosette, J., Palace, M., Cook, B.D., et al. (2014). Amazon forests maintain consistent canopy structure and greenness during the dry season. *Nature, 506,* 221-224.

Nepstad, D.C., Decarvalho, C.R., Davidson, E.A., Jipp, P.H., Lefebvre, P.A., Negreiros, G.H., et al. (1994). The Role of Deep Roots in the Hydrological and Carbon Cycles of

659 Amazonian Forests and Pastures. *Nature, 372,* 666-669.

660 Owe, M., de Jeu, R., & Holmes, T. (2008). Multisensor historical climatology of
661 satellite-derived global land surface moisture. *Journal of Geophysical Research: Earth*
662 *Surface, 113,* F01002, doi: 10.1029/2007JF000769.

663 Owe, M., de Jeu, R., & Walker, J. (2001). A methodology for surface soil moisture and
664 vegetation optical depth retrieval using the microwave polarization difference index.
665 *IEEE Transactions on Geoscience and Remote Sensing, 39,* 1643-1654.

666 Pan, Y.D., Birdsey, R.A., Fang, J.Y., Houghton, R., Kauppi, P.E., Kurz, W.A., et al. (2011). A
667 large and persistent carbon sink in the world's forests. *Science, 333,* 988-993.

668 Parinussa, R.M., Yilmaz, M.T., Anderson, M.C., Hain, C.R., & de Jeu, R.A.M. (2014). An
669 intercomparison of remotely sensed soil moisture products at various spatial scales over
670 the Iberian Peninsula. *Hydrological Processes, 28,* 4865-4876.

671 Phillips, O.L., Aragao, L.E.O.C., Lewis, S.L., Fisher, J.B., Lloyd, J., Lopez-Gonzalez, G., et al.
672 (2009). Drought Sensitivity of the Amazon Rainforest. *Science, 323,* 1344-1347.

673 Platnick, S., *et al.* (2015) MODIS Atmosphere L3 Monthly Product. NASA MODIS Adaptive
674 Processing System, Goddard Space Flight Center, USA.

675 Quesada, C.A., Lloyd, J., Anderson, L.O., Fyllas, N.M., Schwarz, M., & Czimczik, C.I.
676 (2011). Soils of Amazonia with particular reference to the RAINFOR sites.
677 *Biogeosciences, 8,* 1415-1440.

678 Quesada, C.A., Lloyd, J., Schwarz, M., Patiño, S., Baker, T.R., Czimczik, C., et al. (2010).
679 Variations in chemical and physical properties of Amazon forest soils in relation to their

genesis. *Biogeosciences, 7,* 1515-1541.

Rowland, L., da Costa, A.C.L., Galbraith, D.R., Oliveira, R.S., Binks, O.J., Oliveira, A.A.R., et al. (2015). Death from drought in tropical forests is triggered by hydraulics not carbon starvation. *Nature, 528,* 119-122.

Saatchi, S., Asefi-Najafabady, S., Malhi, Y., Aragão, L.E.O.C., Anderson, L.O., Myneni, R.B., et al. (2012). Persistent effects of a severe drought on Amazonian forest canopy. *Proceedings of the National Academy of Sciences of the United States of America, 110,* 565-570.

Saleska, S.R., Didan, K., Huete, A.R., & da Rocha, H.R. (2007). Amazon forests green-up during 2005 drought. *Science, 318,* 612.

Saleska, S.R., Wu, J., Guan, K., Araujo, A.C., Huete, A., Nobre, A.D., et al. (2016). Dry-season greening of Amazon forests. *Nature, 531,* E4-E5.

Samanta, A., Ganguly, S., Hashimoto, H., Devadiga, S., Vermote, E., Knyazikhin, Y., et al. (2010). Amazon forests did not green-up during the 2005 drought. *Geophysical Research Letters, 37,* L05401, doi:10.1029/2009GL042154.

Santi, E. (2010). An application of the SFIM technique to enhance the spatial resolution of spaceborne microwave radiometers. *International Journal of Remote Sensing, 31,* 2419-2428.

Seager, R., Hooks, A., Williams, A.P., Cook, B., Nakamura, J., & Henderson, N. (2015). Climatology, Variability, and Trends in the U.S. Vapor Pressure Deficit, an Important Fire-Related Meteorological Quantity. *Journal of Applied Meteorology and Climatology,*

54, 1121-1141.

Swenson, S., & Wahr, J. (2006). Post-processing removal of correlated errors in GRACE data. *Geophysical Research Letters, 33,* L08402, doi: 10.1029/2005GL025285.

Ten Hoeve, J.E., Remer, L.A., Correia, A.L., & Jacobson, M.Z. (2012). Recent shift from forest to savanna burning in the Amazon Basin observed by satellite. *Environmental Research Letters, 7,* 024020, doi:10.1088/1748-9326/7/2/024020.

Toomey, M., Roberts, D.A., Still, C., Goulden, M.L., & McFadden, J.P. (2011). Remotely sensed heat anomalies linked with Amazonian forest biomass declines. *Geophysical Research Letters, 38,* L19704, doi:10.1029/2011GL049041.

Wielicki, B.A., Barkstrom, B.R., Harrison, E.F., Lee, R.B., Louis Smith, G., & Cooper, J.E. (1996). Clouds and the Earth's Radiant Energy System (CERES): An Earth Observing System Experiment. *Bulletin of the American Meteorological Society, 77,* 853-868.

Wu, J., Albert, L.P., Lopes, A.P., Restrepo-Coupe, N., Hayek, M., Wiedemann, K.T., et al. (2016). Leaf development and demography explain photosynthetic seasonality in Amazon evergreen forests. *Science, 351,* 972-976.

Xu, L.A., Samanta, A., Costa, M.H., Ganguly, S., Nemani, R.R., & Myneni, R.B. (2011). Widespread decline in greenness of Amazonian vegetation due to the 2010 drought. *Geophysical Research Letters, 38,* L07402, doi:10.1029/2011GL046824, 2011

Yan, K., Park, T., Yan, G., Chen, C., Yang, B., Liu, Z., et al. (2016a). Evaluation of MODIS LAI/FPAR Product Collection 6. Part 1: Consistency and Improvements. *Remote Sensing, 8,* 359.

Yan, K., Park, T., Yan, G., Liu, Z., Yang, B., Chen, C., et al. (2016b). Evaluation of MODIS LAI/FPAR Product Collection 6. Part 2: Validation and Intercomparison. *Remote Sensing, 8,* 460.

Zhou, L., Tian, Y., Myneni, R.B., Ciais, P., Saatchi, S., Liu, Y.Y., et al. (2014). Widespread decline of Congo rainforest greenness in the past decade. *Nature, 509,* 86-90.

LIST OF FIGURE CAPTIONS

Fig 1. Spatial distribution of vegetation characteristics over the study area. (a) Land cover map (at 0.10 °spatial resolution) over Amazonia based on the 0.05 °MODIS IGBP classification product for 2010. 'Intact forest' means that all four 0.05° grid cells in one 0.10° grid cell are classified as forest. (b) The 'intact forest' in southern Amazonia (2.5°S–12.5 °S, 75 °W–50 °W as outlined) is the study area of this paper. The annual average VOD value at 0.10 °spatial resolution is displayed in the background. A brief comparison between the downscaled (0.10 °) and original (0.25 °) VOD data can be found in Fig. S1.

Fig 2. Hydrometeorological dynamics over southern Amazonia during non-drought years. Seasonal cycles of rainfall (P, mm $month^{-1}$), photosynthetically active radiation (PAR, W m^{-2}), aerosol optical depth (AOD), cloud optical thickness (COT), terrestrial water storage (TWS, mm), land surface temperature (LST, K) and vapor pressure deficit (VPD, kPa) over the intact forest region in southern Amazonia during non-drought years (i.e., averaged over 2003–2010, excluding 2005 and 2010). The anomalies in 2005 and 2010 will be examined in detail over the extended dry season (May–October) that is outlined by the blue box.

Fig 3. Hydrometeorological anomalies over southern Amazonia in the 2005 and 2010 droughts. Time series of monthly average (a) rainfall (P), (b) photosynthetically active radiation (PAR), (c) aerosol optical depth (AOD), (d) cloud optical thickness (COT), (e) terrestrial water storage (TWS), (f) land surface temperature (LST) and (g) vapor pressure deficit (VPD) over southern Amazonia from May through October in 2005 and 2010 in comparison with non-drought years, respectively.

Fig 4. Anomalies in rainfall (P, mm) and photosynthetically active radiation (PAR, W m^{-2}) for the onset of drought during the wet-to-dry season (May–July) and the peak of drought during the dry season (August–September) of 2005 and 2010. Anomalies represent the departure from the average of non-drought years. The areas with statistically significant anomalies based on non-parametric Wilcoxon signed rank test (p<0.05) are hatched.

Fig 5. Standardized anomalies in vegetation indicators during the onset of droughts (May–July) in 2005 and 2010. Units represent the number of standard deviations as a departure from the average of non-drought years in (a and b) night-time vegetation optical depth (VOD), (c and d) leaf area index (LAI), and (e and f) enhanced vegetation index (EVI). Areas with statistically significant anomalies based on the non-parametric Wilcoxon signed rank test (p<0.05) are hatched.

Fig 6. (a and b) Mean TWS over May–July minus TWS_{MIN} during the non-drought years for each grid cell (ΔTWS). (c and d) Mean LST over May–July minus LST_{MAX} during the non-drought years (ΔLST). (e and f) Mean VPD over May–July minus VPD_{MAX} during the non-drought years (ΔVPD).

Fig 7. Standardized anomalies in night-time VOD during the peak of droughts (August–October) in 2005 and 2010. Units represent the number of standard deviations as a departure from the average of non-drought years. Areas with statistically significant anomalies based on non-parametric Wilcoxon signed rank test (p<0.05) are hatched.

Fig 8. (a and b) Mean TWS over August–October minus TWS_{MIN} during the non-drought years for each grid cell (ΔTWS). (c and d) Mean LST over August–October minus LST_{MAX}

during the non-drought years (ΔLST). (e and f) Mean VPD over August–September minus VPD_{MAX} during the non-drought years (ΔVPD). (g and h) Total number of months with monthly rainfall below 100 mm and significantly below average of non-drought years, between May and October in 2005 and 2010 respectively for each grid cell.